Supporting Information

Alexandra Lamtyugina, Yuqing Qiu, Étienne Fodor, Aaron R. Dinner, Suriyanarayanan Vaikuntanathan

S1. METHODS

A. Cytosim simulations

We perform simulations using Cytosim [1]. We make modifications to the Cytosim source code pertaining to simulation data output to access quantities which are not output by the built-in report functions. Source code for these modifications is available upon request. This modified version of Cytosim used for all simulations was compiled into a Singularity container [2], which is also available upon request. All simulations are in 2D without periodic boundary conditions and we tabulate all simulation parameters in the SI (Sec. S4).

The persistence length L_p of the filaments is related to the filament rigidity through `rigidity` $= k_B T L_p$, where k_B is the Boltzmann constant and T is the temperature. At the temperature in our simulations ($k_B T = 1$), the persistence length is 0.1 µm, which indicates that the filaments of length 0.25 µm are semi-flexible in nature. Refer to Table S2 in Sec. S4 for detailed simulation parameters.

B. Filament orientations in asters and bundles

Fig. S1 demonstrates the orientations of filaments in the structures observed during simulations at various values of motor stiffness k. Lower values of k (top frames) correspond to asters, where filaments are radially distributed and point towards the center of the structure. Larger values of k (bottom right frame) results in bunle-like structures with anti-parallel orientation of the filaments along its long axis.

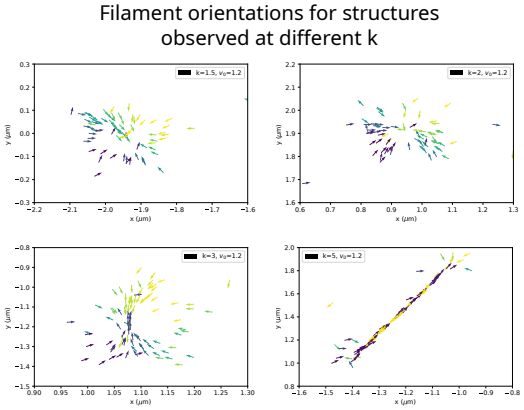

Figure S1: Filament orientations at various values of k.

C. Radius of gyration of filament clusters

We calculate the radius of gyration $R_g(v_0, k)$ of the actin structures in the unbiased simulations. First, we use motor connectivity to identify filaments that belong to the largest cluster as reported by Cytosim. We calculated the radius of gyration of the largest cluster as

$$R_g(v_0, k) = \sqrt{\frac{1}{N}\sum_{i=1}^{N} r_i^2} \tag{S1}$$

where r_i is distance between the center of mass of filament i and the center of mass of the largest cluster. For each combination of v_0 and k, we perform 500 independent unbiased simulations of 100 s each, and compute $R_g(v_0, k)$ from the last frame of these trajectories, as well as its error bar.

The radius of gyration as a function of motor rigidity k exhibits the same behavior for various values of v_0.

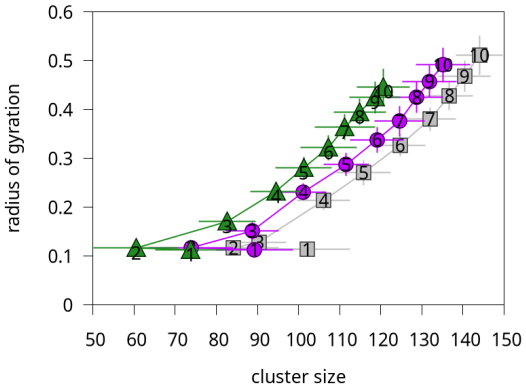

Figure S2: R_g as a function of cluster size for unloaded speeds $v_0 = 0.8$ (gray), 1.0 (magenta) and 1.2 (green). k values are listed inside the symbols.

D. Computing rate of work of motors

The rate of work is calculated from the output data generated by Cytosim. We extract the force exerted by each doubly-bound motor and the direction of movement of each motor head, and calculate the magnitude of velocity of each motor head according to the force-velocity relationship (**??**). The rate of work $\dot{w}$ for each motor head is then calculated using **??**. Note that each motor force is always pointing from the motor head to the center of the motor. The values of $\langle \dot{w} \rangle$ in **??**(b) are time averages of the total $\dot{w}$ performed by all doubly-bound motors in the system. We run 100 independent 100 s trajectories for each parameter combination, and take the $\dot{w}$ average over the last 30 s of each trajectory.

E. Trajectory biasing through the cloning algorithm

Trajectory biasing, the primary technique in our work, is based on the theory of large deviations. Observables for a system will exhibit some average value (taken over some time period τ) for an ensemble of trajectories. In this case, a single trajectory is a sequence of states for a system of filaments and motors which evolve according to the dynamics defined by the Cytosim simulation engine. Occasionally, a single trajectory may exhibit a value for an observable that is very far from the ensemble average. Large deviations theory provides an estimate of the probability of the rare event that the observable will take on a value that is significantly different from the average [3]. For the sake of brevity, we bypass much of the mathematical description of the theory of large deviations in favor of describing how we apply this theory in the context of our work. For a more rigorous description of the mathematics, refer to the references cited herein.

An established approach to "amplify" the occurrence of rare events [4] is through controlling the probabilities of deviations of some observable A from its ensemble average $\bar{A}$ via a biasing field. In our case, the biasing field is denoted by α, and the observable A is $\frac{1}{\tau}\int_0^\tau \dot{w}\, dt$. The bias is applied by modifying the probability of each trajectory with an exponential term:

$$P_\alpha \propto P_0 \exp[-\alpha \tau A] = P_0 \exp\left[-\alpha \int_0^\tau \dot{w}\, dt\right]. \tag{S2}$$

As a result, we are able to more effectively generate rare trajectories which correspond to large fluctuations in the value of $\dot{w}$ from the average. Moreover, we can draw a quantitative connection between the strength of the bias that we apply, α, and the resulting arrangement of filaments. As discussed in [4], it is reasonable to consider a scenario in which changes in the probabilities of rare events are a result of some external or internal driving force.

We use the cloning algorithm to perform importance sampling on trajectories obtained from the Cytosim simulations. The cloning algorithm procedure follows closely the one described in Ref. [3]. To briefly summarize the

procedure, the native Cytosim code was used to create multiple clones. These are propagated for a time period τ, chosen to be longer than the autocorrelation time of the system (calculated using the `statsmodel.tsa.stattools` Python package [5]). Depending on the calculated values of $\dot{w}$ of individual trajectories, clones are either "killed" or allowed to "proliferate" and are duplicated to replace the eliminated clones. Cytosim is then used to propagate the equations of motion for time τ, and the process is repeated. In other words, in order to perform the biasing simulations and extract the large deviation statistics, we integrated the cloning algorithm with the Cytosim package. The source code for our implementation the cloning algorithm can be found at `https://github.com/alamda/cytosim-cloning-algorithm`.

F. Distribution of $\sin\theta$

We define an order parameter $\sin\theta$ to quantify the relative alignment of neighboring filaments, where θ is the angle between filament pairs in the largest cluster. We first find the number of filament neighbours for each filament within a distance cutoff of $d = 0.25$ µm (equal to the length of a single filament), where the distance between a filament pair is computed as the distance between the two positive ends of the filaments. If a filament has more than $n = 40$ neighbours, we consider it to be a part of the largest cluster. We then compute $\sin\theta$ of the center filament with respect to its 40 closest neighbours, and the average $\sin\theta$ is taken over these 40 filament pairs for each center filament. The $\sin\theta$ distribution is generated from the $\sin\theta$ values for every filament belonging to a cluster.

Reference curves for $v_0 = \{0.8, 1.0, 1.2\}$ µm s^{-1} are generated from the last frame of 500 independent trajectories, each 100 s long. The $\sin\theta$ distributions from cloning simulations are generated from the last snapshot of each surviving clones at the end of each iteration, starting from the 6^{th} iteration (thus discarding the first 150 s of each cloning trajectory). If the surviving clone is copied n times at the end of the iteration, the statistics of structure from its last frame is also copied n times when generating the $\sin\theta$ histogram.

The $\sin\theta$ histogram is related to the radius of gyration R_g, but not equivalent. $P(\sin\theta)$ provides a better description of the statistics of structure of the assemblies. We compare the radius of gyration R_g and the average of $\sin\theta$ for various motor rigidity k (Fig. S3). R_g increases almost linearly with increasing k as the bundles become longer. $\langle\sin\theta\rangle$ decreases with increasing k because the filaments are more aligned in the bundles. $\langle\sin\theta\rangle$ has better resolution when the transition between aster to bundle occurs near $k = 3$. Therefore, we use R_g for the phase diagram and focus on $P(\sin\theta)$ for analyzing the structures when the biasing is applied.

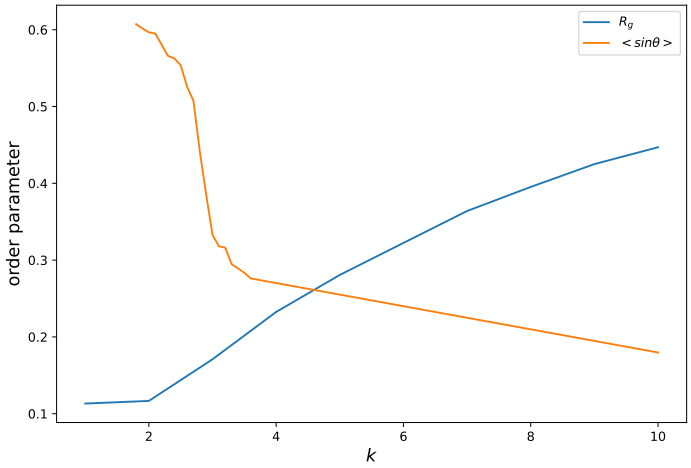

Figure S3: R_g and $\langle\sin\theta\rangle$ for various motor rigidity k with $v_0 = 1.2$.

G. Extracting k_{eff} from biased simulations

We use the order parameter statistics in the biased dynamics $P_\alpha(\sin\theta)$ to characterize the assembly structure obtained as a result of dynamical bias. The value of the effective rigidity k_{eff} corresponding to each biasing factor α is extracted with the following procedure. We measure $P(\sin\theta)$ in the unbiased dynamics for a set of k values between

$k_0 - 0.5$ and $k_0 + 0.5$ with an increment of 0.05, where k_0 is the rigidity value used in the biased dynamics. Then, we compute the Kullback-Leilbler divergence between $P_\alpha(\sin\theta)$ and each of the reference distributions $P(\sin\theta)$, defined as

$$\mathcal{D}_{KL}(P_\alpha||P) = \sum_{\sin\theta} P_\alpha(\sin\theta)\log\frac{P_\alpha(\sin\theta)}{P(\sin\theta)}. \tag{S3}$$

It measures the difference between the statistics of structures from the biased and unbiased dynamics. The reference distribution with k that gives the minimum value of relative entropy leads to $k_{\text{eff}} = k$. We generate five independent sets of reference curves $P(\sin\theta)$ for each combination of v_0 and k_0. Each reference curve is generated by analyzing the structures from 100 independent trajectories and each of the trajectories runs for 3000 s. We compute k_{eff} using each set of these reference curves and the error bars of k_{eff} from these five sets (**??**(e)).

S2. HYDRODYNAMIC MODEL AND MEAN-FIELD TREATMENT OF DYNAMICAL BIAS

A. A minimal hydrodynamic model of the actomyosin system

In order to investigate how trajectory biasing might renormalize material properties, we consider a minimal hydrodynamic model of the actomyosin system governed by the equations in Ref. [6]:

$$\partial_t\rho = -\nabla\cdot[v_0\rho\vec{n} - D\nabla\rho], \tag{S4}$$

$$\partial_t\vec{n} = K_1\nabla^2\vec{n} + K_2\nabla[\nabla\cdot\vec{n}] + \xi\nabla[\rho] + \alpha\vec{n} - \beta|\vec{n}|^2\vec{n}, \tag{S5}$$

where ρ is the density of the actin filaments, and $\vec{n}$ is a polar field which represents the orientation of the filaments. The effects due to motor activity are implicitly accounted for in this minimal model. Equation S4 captures the changes to filament density (ρ) due to advection and diffusion. Equation S5 characterizes the time-dependent behavior of the filament director field ($\vec{n}$). K_1 and K_2 terms capture the nematic behavior of the filaments, whereas the α and β terms control the order-disorder transition of the system. The ξ term accounts for the reorientation of $\vec{n}$ along gradients of ρ, thus capturing the non-equilibrium effects due to motor activity. In particular, as detailed in Ref. [6], we expect ξ to be inversely correlated to the motor rigidity. The parameter α is expected to be positively correlated with the rigidity of the motor and its ability to crosslink actin filaments. These minimal equations of motion can be used to recover many of the biophysically observed configurations, such as asters and bundle like objects.

The transition from an isotropic phase to an aster like phase is particularly amenable to analytical treatment. Indeed, performing linear stability analysis on Eq. (S4) and Eq. (S5), and keeping track of the fastest growing mode following the procedure detailed in Ref. [7], we can reformulate the equations for ρ, v_0, ξ, and α: $\rho = \rho_0 + \epsilon\rho_1$, $v_0 = v_0^{(0)} + \epsilon v_1$, $\xi = \xi_0 + \epsilon\xi_1$, $\alpha = \alpha_0 + \epsilon\alpha_1$, where $\epsilon \ll 1$. The parameters $v_0^{(0)}$, ξ_0, and α_0 denote the values at which the homogeneous phase first becomes unstable, given by $D + \xi_0 v_0^{(0)}/\alpha_0 = 0$, and ρ_0 is the density of the actin in the homogeneous phase. The effective dynamics for ρ_1 is the given by

$$\partial_t\rho_1 = b\nabla^2\rho_1 - c\nabla(\rho_1\nabla\rho_1) - \lambda\nabla^4\rho_1 \equiv \nabla^2\left(\frac{\delta F}{\delta\rho_1}\right), \tag{S6}$$

where $b \equiv v_0^1\rho_0\xi_0/\alpha_0$ and $c \equiv v_0\xi_0/\alpha_0$ depend on motor properties properties ξ, v_0, α. In other words, the evolution of the density field can be described using an effective free energy F that can be written as

$$F = \int d\vec{r}\left[f(\rho) + \frac{\lambda}{2}(\nabla\rho)^2\right], \quad f(\rho) = \frac{b}{2}\rho^2 - \frac{c}{3!}\rho^3. \tag{S7}$$

This effective free energetic landscape permits multiple metastable solutions depending on the value of ξ. While our analytical arguments only lead to quadratic and cubic terms in the effective free energy landscape, packing constraints can be expected to lead to a quartic term with a positive coefficient. Similarly, reflecting a finite chemical potential, we may also expect linear term in the effective free energy landscape.

B. Mean-field treatment of dynamical bias

Inspired by the result presented in Eq. S7, we use a similar form of the free energy to evaluate the effect of a dynamical bias on the phenomenological constants a, b, c, and d and any corresponding material properties. We examine a phenomenological model by writing down the dynamics of a structural order parameter ψ. We consider that the landscape describing the statistics of this order parameter has a Landau-like form [3], that under the appropriate conditions permits two metastable solutions: $\mathcal{F}(\psi) = -a\psi + b\psi^2 - c\psi^3 + d\psi^4$, with $\{a, b, c, d\}$ as phenomenological parameters. Even for systems with underlying non-equilibrium dynamics, such a landscape can be obtained for the dynamics of reduced order parameters, where first order transitions can be accessed by modulating the minimum of the landscape [7]. The parameter controlling such a transition is meant to capture the behavior observed in our system where tuning the rigidity k results in a structural transition from isotropic phase to asters.

Within such a framework, we consider that the dynamics of the structural order parameter ψ reads

$$\dot{\psi} = -\partial_\psi \mathcal{F}(\psi) + \sqrt{2D}\zeta, \tag{S8}$$

where ζ is Gaussian white noise with zero mean and D is the noise strength. At leading order in D, the Onsager-Machlup action $\mathcal{A}$ which determines the path probability $\mathcal{P} \sim e^{-\mathcal{A}/D}$ of the dynamics of ψ [3] reads,

$$\mathcal{A} = \frac{1}{4}\int_0^t (\dot{\psi} + \partial_\psi \mathcal{F}(\psi))^2 \, ds. \tag{S9}$$

If we apply a bias on a function of the order parameter ψ, which we define as $g(\psi)$, the action $\mathcal{A}_\alpha$ associated with this biased dynamics is given by

$$\mathcal{A}_\alpha = \frac{1}{4}\int_0^t (\dot{\psi} + \partial_\psi \mathcal{F}(\psi))^2 \, ds - \int_0^t (\alpha g(\psi) + \Phi(\alpha)) \, ds, \tag{S10}$$

where $\Phi(\alpha)$ is the scaled cumulant generating function, $\Phi(\alpha) = \lim_{t\to\infty} \frac{D}{t} \ln\langle \exp^{(\alpha/D)\int_0^t g(\psi)\, ds}\rangle$. At small D, this term can be written as $\Phi(\alpha) = -\frac{1}{4}\min_\psi[\partial_\psi \mathcal{F}(\psi)^2 - 4\alpha g(\psi)]$ [3]. We introduce the action $\mathcal{A}_{\text{eff}}$ for the effective dynamics as

$$\mathcal{A}_{\text{eff}} = \frac{1}{4}\int_0^t (\dot{\psi} + \partial_\psi \mathcal{F}_{\text{eff}}(\psi))^2 \, ds. \tag{S11}$$

The corresponding effective free energy landscape then can be written as

$$\partial_\psi \mathcal{F}_{\text{eff}}(\psi) = \sigma(\psi)\sqrt{\partial_\psi \mathcal{F}(\psi)^2 - 4[\alpha g(\psi) + \Phi(\alpha)]}, \tag{S12}$$

where $\sigma = 1$ for $\psi < \bar{\psi}$ ($\sigma = -1$ otherwise), and at small D, $\bar{\psi}$ can be determined as $\bar{\psi} = \arg\min_\psi[\partial_\psi \mathcal{F}(\psi)^2 - 4\alpha g(\psi)]$ [3, 8]. Note that $\mathcal{A}_{\text{eff}}$ in Eq. (S11) coincides with $\mathcal{A}_\alpha$ in Eq. (S10) up to a boundary term that is irrelevant for the trajectory weights. If we consider $g(\psi) = 0.1\psi$ and take a free energy $\mathcal{F}$ with a global minimum at $\psi > 0$, we can generate the corresponding modified free energy $\mathcal{F}_{\text{eff}}(\psi)$ that changes minimum for $\alpha > 0$ through numerical means. Fig. S4 shows the effective free energy landscape when various biasing α are applied. We fit the effective free energy $F_{\text{eff}}(\psi)$ to extract the effective phenomenological parameters b_{eff} and c_{eff}, and find that applying the biasing leads to changes in the quadratic and cubic terms of the effective free energy. The associated probability distribution $P(\psi)$, proportional to $e^{-\mathcal{F}_{\text{eff}}(\psi)/D}$ up to normalization factor, is shown in Fig. **??**(d) in the main text. This simple perturbative analysis reveals that the structural transition in the effective free energy landscape is obtained by tuning α (Table S1).

Table S1: Renormalized phenomenological parameters at various α

α	b_{eff}	c_{eff}
0	-1	-0.033
0.005	-0.96	-0.003
0.1	-0.91	0.046
0.3	-0.84	0.108

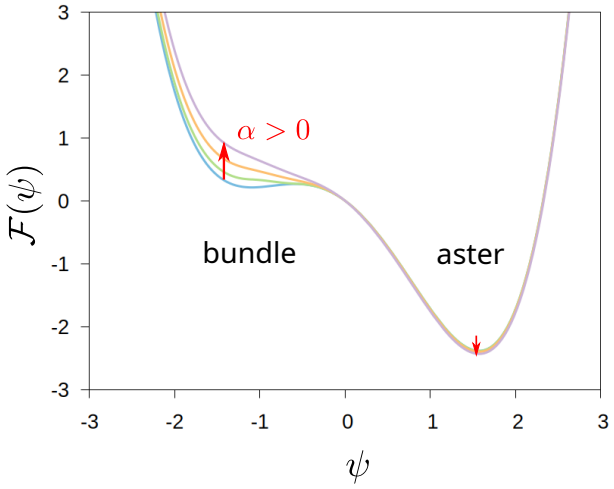

Figure S4: Free energy landscapes obtained by biasing the dynamics with respect to ψ. The original free energy has the form $\mathcal{F}(\psi) = -a\psi + b\psi^2 - c\psi^3 + d\psi^4$. Values of α: $\alpha = 0$ (unbiased dynamics, blue), 0.005 (green), 0.1 (orange) and 0.3 (purple). Other parameters are $a = 4d = -b = -30c = 1$.

S3. DERIVATION OF THE TWO-STATE MODEL AND PREDICTION OF k_{eff}

A. Model description

The minimal two-state model is intended to capture the effect of an applied bias on the probabilities of aster and bundle states. We characterize the two states through the order parameter $P(\sin\theta)$ and the average values of the rate of work $\langle\dot{w}\rangle$, both of which exhibit a dependence on k. These values serve as inputs to the two-state model to construct a curve predicting the relationship between the strength of the applied bias α and k_{eff}.

For an unbiased system, we describe the dynamics through the master equation $\dot{P} = \boldsymbol{W}P$, where P is a vector containing the original probabilities of the two states $\{P_{\text{aster}}, P_{\text{bundle}}\}$, and the transition rate matrix $\boldsymbol{W}$ is given in equation (**??**). We assign relative energies $\varepsilon_{\{\text{aster, bundle}\}}$ to each state in order to evaluate the transition rates between asters and bundles ($R_{ab} = A\exp[-\beta\varepsilon_{\text{bundle}}]$ and $R_{ba} = A\exp[-\beta\varepsilon_{\text{aster}}]$). For convenience, we work in units where $A = 1$, $\beta = 1/(k_BT) = 1$, and we set $\varepsilon_{\text{bundle}} = 0$.

When biasing is applied to trajectory probabilities, the new transition rate matrix $\boldsymbol{W}^{(\alpha)}$ takes the form shown in equation (**??**). There it is clear that the biasing factor alters the transition rates between the two states by an amount proportional to the biasing strength and the rate of work of each state. Using values extracted from unbiased simulations ($\varepsilon_{\{\text{a,b}\}}$ and $\dot{w}_{\{\text{a,b}\}}$), we can then calculate an effective energy for each state (equation **??**, Section S3 B). By relating the energy levels $\varepsilon_{\{\text{a,b}\}}$ and $\varepsilon^{(\alpha)}_{\{\text{a,b}\}}$ to their respective probability distributions $P_{\{\text{a,b}\}}$ and $P^{(\alpha)}_{\{\text{a,b}\}}$ (equation (**??**)), the two-state model illustrates the effect of an applied bias on the dynamics, and therefore the structural configuration of the system.

The biased transition rate matrix $\boldsymbol{W}^{(\alpha)}$ is also known as a "tilted" matrix, and is constructed based on the principles of the theory of large deviations [9, 10]. The cumulant generating function is obtained by taking the logarithm of the largest eigenvalue of $\boldsymbol{W}^{(\alpha)}$. By construction, $\boldsymbol{W}^{(\alpha)}$ is not normalized, otherwise the eigenvalue (and thus the cumulant generating funciton) would be zero, which would be inconsistent with the presence of a bias.

Figure S5 illustrates the two state model.

B. Derivation of the left eigenvector of Eq. 7

We define the left eigenvector of $\boldsymbol{W}^{(\alpha)}$ as $\begin{bmatrix} a & 1 \end{bmatrix}$:

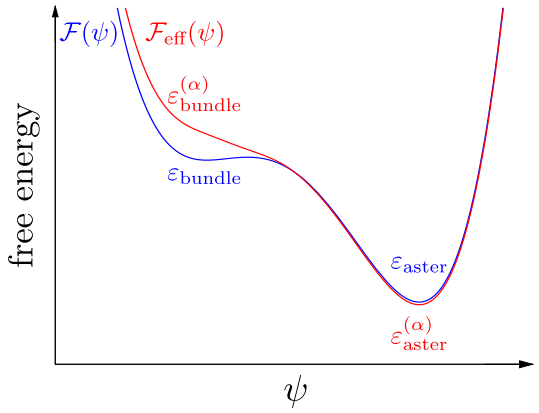

Figure S5: Schematic of the two state model. Blue curve is the free energy of the original dynamics, red curve is the free energy in the presence of trajectory biasing.

$$\begin{bmatrix} a & 1 \end{bmatrix} \boldsymbol{W}^{(\alpha)} = \begin{bmatrix} a & 1 \end{bmatrix} \begin{bmatrix} -R_{ab} + \alpha \dot{w}_{\text{aster}} & R_{ba} \\ R_{ab} & -R_{ba} + \alpha \dot{w}_{\text{bundle}} \end{bmatrix} = \epsilon \begin{bmatrix} a & 1 \end{bmatrix}, \tag{S13}$$

where ϵ is the corresponding eigenvalue. The transition rates can be computed from the energies of aster $\varepsilon_{\text{aster}}$ and bundle $\varepsilon_{\text{bundle}}$, *i.e.*, $R_{ab} = A \exp[-\beta \varepsilon_{\text{bundle}}]$ and $R_{ba} = A \exp[-\beta \varepsilon_{\text{aster}}]$. We select $A = 1$ and $k_B T = 1$ and set $\varepsilon_{\text{bundle}} = 0$ for convenience. Hence, the matrix above becomes

$$\begin{bmatrix} a & 1 \end{bmatrix} \boldsymbol{W}^{(\alpha)} = \begin{bmatrix} a & 1 \end{bmatrix} \begin{bmatrix} -1 + \alpha \dot{w}_{\text{aster}} & R_{ba} \\ 1 & -R_{ba} + \alpha \dot{w}_{\text{bundle}} \end{bmatrix} = \epsilon \begin{bmatrix} a & 1 \end{bmatrix}, \tag{S14}$$

We solve Eq. (S14) and find that $\ln a$ can be expressed in terms of α, $\dot{w}_{\text{aster}}$ and R_{ba} as

$$\begin{aligned} a =& \frac{(R_{ba} - 1) + \alpha \Delta \dot{w} + \sqrt{(R_{ba} - 1 + \alpha \Delta \dot{w})^2 + 4 R_{ba}}}{2 R_{ba}} \\ \approx& \frac{(R_{ba} - 1) + \alpha \Delta \dot{w} + \sqrt{(R_{ba} + 1 + \frac{R_{ba}-1}{R_{ba}+1} \alpha \Delta \dot{w})^2}}{2 R_{ba}} + \mathcal{O}(\alpha^2) \\ \approx& 1 + \frac{\alpha \Delta \dot{w}}{1 + R_{ba}} + \mathcal{O}(\alpha^2), \end{aligned} \tag{S15}$$

where $\Delta \dot{w} = \dot{w}_{\text{aster}} - \dot{w}_{\text{bundle}}$, and $\dot{w}_{\text{aster}}$ and $\dot{w}_{\text{bundle}}$ are the rate of work for aster state and bundle state as defined in Eq. 2 (main text). According to Doob theorem [11], the left eigenvector of $\boldsymbol{W}^{(\alpha)}$ contains the information of the correction to the energy landscape of $\varepsilon_{\text{aster}}$.

$$\varepsilon^{(\alpha)}_{\text{aster}} \approx \varepsilon_{\text{aster}} - \ln a \approx \varepsilon_{\text{aster}} - \ln\left(1 + \frac{\alpha \Delta \dot{w}}{1 + R_{ba}} + \mathcal{O}(\alpha^2)\right) \approx \varepsilon_{\text{aster}} - \frac{\alpha \Delta \dot{w}}{1 + R_{ba}} + \mathcal{O}(\alpha^2). \tag{S16}$$

Eq. (S16) is the same as Eq. 7 in the main text. Since $\Delta \dot{w} > 0$ as shown in Fig. 1(c), Eq. (S16) indicates that applying a positive α lowers the energy of aster state (Fig. 2(e)).

C. k_{eff} predicted by the two-state model

We use Eq. 7 derived above to predict k_{eff} from the two-state model. We first build a relation between $\varepsilon_{\text{aster}}$ and k using the metric $\sin\theta$. We carry out unbiased simulations for the full range of the motor rigidities k and calculate their corresponding distribution $P(\sin\theta)$. We then compute the probability of aster P_{aster} at each k with the following

expression

$$P_{\text{aster}} = \int_{0.6}^{1} P(\sin\theta)\, d\sin\theta. \tag{S17}$$

The quantity P_{aster} is then used to estimate the energy of aster for each k using

$$\varepsilon_{\text{aster}} = -\ln \frac{P_{\text{aster}}}{1 - P_{\text{aster}}}. \tag{S18}$$

Eq. (S18) enables us to construct a reference curve of $\varepsilon_{\text{aster}}$ as a function of motor rigidity k for each unloaded velocity v_0. As we have shown in the biased simulations of Cytosim, applying an α bias is equivalent to tuning k. In principle, we can then connect α with the effective rigidity k_{eff} through the relation

$$\varepsilon^{(\alpha)}_{\text{aster}}(k) = \varepsilon_{\text{aster}}(k_{\text{eff}}). \tag{S19}$$

To estimate $\varepsilon^{(\alpha)}_{\text{aster}}(k)$ for each biasing parameter α, we need the additional relation in Eq. (S16). Here, we assume further that $\Delta\dot{w}$ is proportional to the slope of the $\langle\dot{w}\rangle$ versus k curve (Fig. S6), as numerically evaluated from the unbiased dynamics of Cytosim. This procedure allows us to extract an analytic relation between α and k_{eff} for each unloaded velocity v_0, as plotted in Fig. 2(e) of the main text.

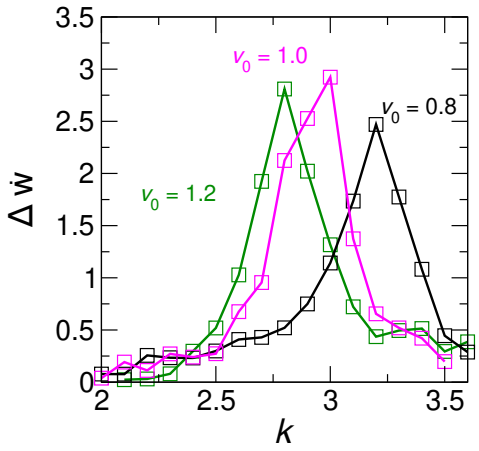

Figure S6: $\Delta\dot{w}$ at $v_0 = 0.8, 1.0, 1.2\ \mu\text{m}\,\text{s}^{-1}$ for motor rigidity k in increments of 0.1.

S4. CYTOSIM SIMULATION PARAMETERS

Parameter name	Parameter value	Units
`time_step`	0.001	s
`viscosity`	0.001	$\mathrm{pN\,s\,\mu m^{-2}}$
`temperature` (k_BT)	1	$\mathrm{pN\,\mu m}$
simulation box size	5×5	$\mathrm{\mu m^2}$
filament `rigidity`	0.1	$\mathrm{pN\,\mu m^2}$
filament `segmentation`	0.1	µm
filament `length`	0.25	µm
number of filaments	200	—
filament confinement	1	$\mathrm{pN\,\mu m^{-1}}$
myosin `binding_rate`	10	$\mathrm{s^{-1}}$
myosin `binding_range`	0.1	µm
myosin `unbinding_rate`	1	$\mathrm{s^{-1}}$
myosin `unbinding_force`	10	pN
myosin `activity`	`move`	(towards actin + end)
myosin `stall_force` (f_0)	10	pN
myosin `unloaded_speed` (v_0)	0.8, 1.0, 1.2	$\mathrm{\mu m\,s^{-1}}$
myosin `stiffness` (k)	0–10	$\mathrm{pN\,\mu m^{-1}}$
myosin rest `length`	0	µm
number of myosin motors	1000	—
rate of work $\dot{w}$	—	$\mathrm{pN\,\mu m\,s^{-1}}$
biasing parameter α	—	$\mathrm{pN^{-1}\,\mu m^{-1}}$

Table S2: Simulation parameters.

S5. CHARACTERIZING THE STRUCTURE OF ACTIN ASTER AND BUNDLE

Fig. S7 illustrates the time-dependent behavior of R_g and cluster size for different combinations of k and v_0. Plots contain points only for structures of at least 40 filaments in size. Plots for $v_0 = 1.8$ are not shown due to the absence of large clusters. Values of R_g and cluster size both reach steady states on the timescales of our simulations.

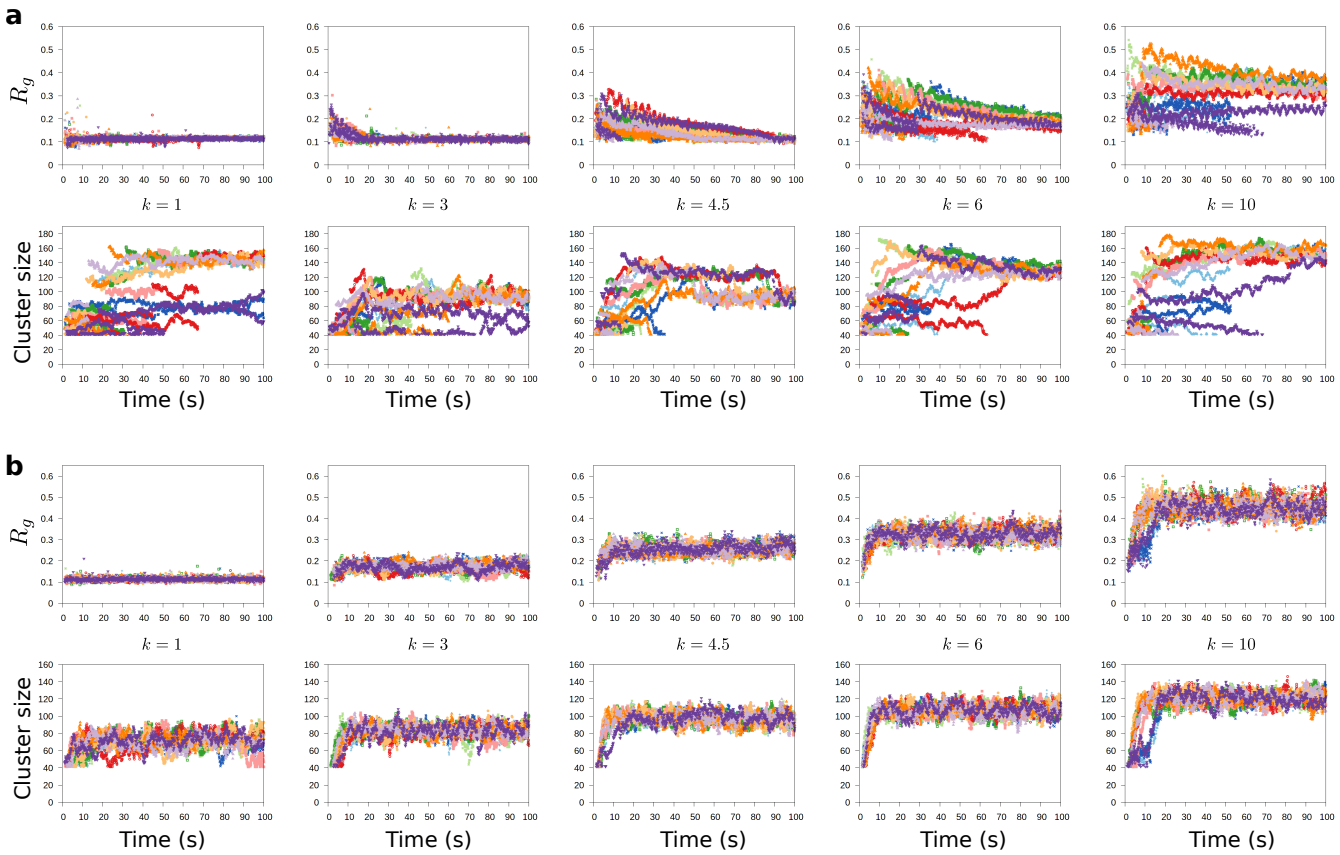

Figure S7: Characterization of steady-state structures. Radius of gyration (top row) and cluster size (bottom row) over time using various values of k for (a) $v_0 = 0.2$ and (b)$v_0 = 1.2$. Only data points corresponding to clusters with more than 40 filaments are shown. For all simulations, the isotropic phase was the starting configuration.

S6. CLONING QUALITY

To qualify the effectiveness of the cloning algorithm, we examine the cloning statistics. This analysis is done by calculating the number of times that the most viable clone is copied among all cloning copies and normalizing that number by the total number of clones N_c. The goal is to avoid a single clone dominating the trajectory space at any given iteration. Satisfactory cloning statistics will yield values close to 0, whereas values close to 1 indicate that the trajectory space sampling is inadequate. Stronger biasing requires larger numbers of clones, as the fluctuations which are to be picked and cloned by large biasing factors are more rare. We determine that the acceptable cloning statistics for $\alpha = \pm 0.05, \pm 0.1, \pm 0.2, \pm 0.3$ and ± 0.4 can be achieved using $N_c = 480, 480, 1440, 19200$ and 19200, respectively. The cloning quality plots in Fig. S8 indicate that the cloning statistics remain away from 1 for $|\alpha| \leq 0.3$.

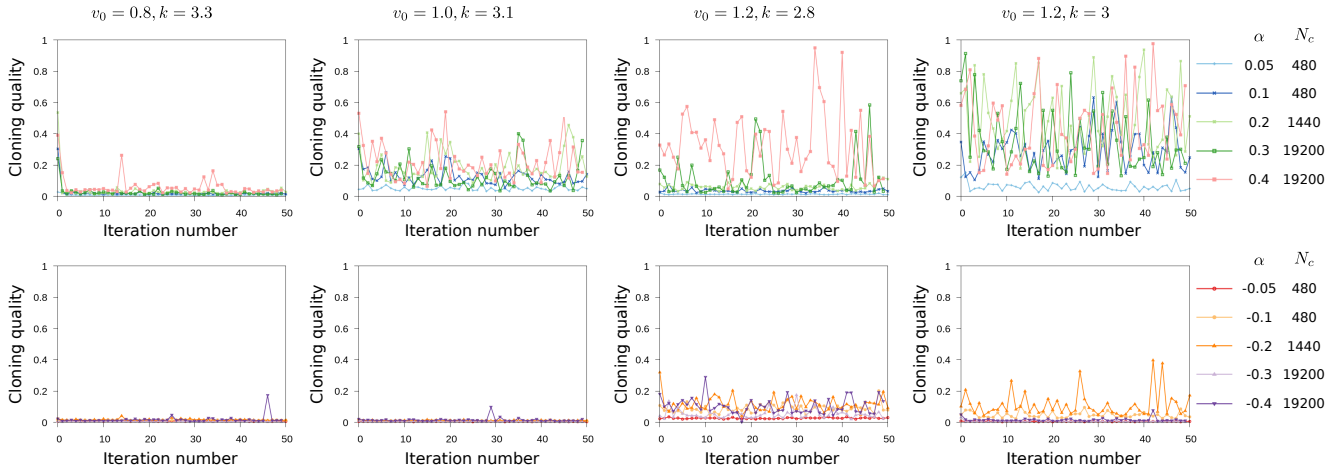

Figure S8: Cloning quality plots.

[1] Francois Nedelec and Dietrich Foethke. Collective Langevin dynamics of flexible cytoskeletal fibers. *New Journal of Physics*, 9(11):427–427, Nov 2007.

[2] Gregory M. Kurtzer, Vanessa Sochat, and Michael W. Bauer. Singularity: Scientific containers for mobility of compute. *PLOS ONE*, 12(5):e0177459, May 2017.

[3] Takahiro Nemoto, Freddy Bouchet, Robert L. Jack, and Vivien Lecomte. Population-dynamics method with a multicanonical feedback control. *Physical Review E*, 93(6):062123, Jun 2016.

[4] R. L. Jack. Ergodicity and large deviations in physical systems with stochastic dynamics. *Eur. Phys. J. B*, 93:74, 2020.

[5] Skipper Seabold and Josef Perktold. statsmodels: Econometric and statistical modeling with python. In *9th Python in Science Conference*, 2010.

[6] Kripa Gowrishankar and Madan Rao. Nonequilibrium phase transitions, fluctuations and correlations in an active contractile polar fluid. *Soft matter*, 12(7):2040–2046, 2016.

[7] Thomas Speck, Julian Bialké, Andreas M. Menzel, and Hartmut Löwen. Effective Cahn-Hilliard equation for the phase separation of active brownian particles. *Phys. Rev. Lett.*, 112:218304, May 2014.

[8] Nicolás Tizón-Escamilla, Vivien Lecomte, and Eric Bertin. Effective driven dynamics for one-dimensional conditioned Langevin processes in the weak-noise limit. *Journal of Statistical Mechanics: Theory and Experiment*, 2019(1):013201, 2019.

[9] Hugo Touchette. The large deviation approach to statistical mechanics. *Physics Reports*, 478(1–3):1–69, Jul 2009.

[10] Hugo Touchette. A basic introduction to large deviations: Theory, applications, simulations. (arXiv:1106.4146), Feb 2012. arXiv:1106.4146 [cond-mat, physics:math-ph].

[11] Joseph L. Doob. *Stochastic processes*. Wiley classics library edition. Wiley, 1990.